Scientia Iranica B (2014) 21(4), 1403–1414

SCIENTIA IRANICA

Sharif University of Technology
Scientia Iranica
Transactions B: Mechanical Engineering
www.scientiairanica.com

Numerical study of mixed convection in the annulus between eccentric rotating cylinders

A. Abedini, A.B. Rahimi* and A. Kianifar

Faculty of Engineering, Ferdowsi University of Mashhad, Mashhad, P.O. Box 91775-1111, Iran.

Received 8 October 2012; received in revised form 21 September 2013; accepted 5 March 2014

KEYWORDS
Mixed convection;
Bipolar-coordinate system;
Annulus;
Constant angular velocity.

Abstract. Mixed convection of air with Prandtl number of 0.7 in eccentric horizontal annuli with isothermal wall conditions was numerically investigated. The inner cylinder was at a higher temperature and the inner and outer cylinders rotate either clockwise or counter-clockwise at a constant angular velocity. The effects of parameters such as the eccentricity of the axes, the Rayleigh number and rotation direction were studied. The two-dimensional Navier-Stokes and energy equations were numerically solved in an orthogonal grid by employing a finite-volume method based on the SIMPLE algorithm. This orthogonality was achieved by employing a cylindrical bipolar coordinate system. Use of this coordinate system has the privileges of orthogonal coordinate and simplicity of computing different fluxes involved. Mean and local heat transfer results were obtained. The physics of the flow and the heat transfer is revealed by the streamlines and the isotherms obtained from the numerical solutions. Flow and heat transfer are influenced by the orientation and eccentricity of the inner cylinder. The present numerical results are in good agreement with the results of others for pure natural convection.

1. Introduction

Mixed convection in the annulus between two cylinders has attracted attention because of its engineering applications such as mixtures, thermal energy storage systems, electrical components cooling, double pipe heat exchangers designed for chemical processes, food industries, and nuclear reactors. Kuehn and Goldstein [1,2] give an overview for concentric and eccentric annuli. They measured the heat transfer coefficients in air and water for natural convection in concentric and eccentric horizontal annuli. Their experimental data are commonly used to validate most of the recent numerical studies. Later, Macleod and Bishop [3] performed several measurements of overall heat transfer rates and profiles of the time-averaged and fluctuating temperature field for fully turbulent natural convection. In some applications to increase the heat transfer rate, fins are used in the axial direction. Chai and Patankar [4], Desrayaud et al. [5], Patankar et al. [6], and Rustum and Soliman [7] investigated the effect of fins attached on the inner and outer cylinders on the fluid flow and heat transfer in annuli by analyzing the result obtained from the numerical solution of the two-dimensional and steady-state governing equations. Shahraki [8] demonstrated the effect of temperature-dependent properties on the streamlines and temperature distributions in a concentric annulus. The varying viscosity had the strongest effect on the flow field while the thermal conductivity had the strongest effect on temperature profiles. Dyko et al. [9] presented numerical and experimental buoyancy driven flow in an annulus between two horizontal coaxial cylinders at Rayleigh numbers exceeding the critical value depending on radius ratio. Alawadhi [10] studied the natural

*. *Corresponding author. Tel: +98 511-8805018*
E-mail addresses: ahad_abedini@yahoo.com (A. Abedini); rahimiab@yahoo.com (A.B. Rahimi); a_kianifar@yahoo.com (A. Kianifar)

convection flow in a horizontal annulus enclosure with a transversely oscillating inner cylinder numerically. Natural convection of a micro-polar fluid in an eccentric annulus enclosure was studied by Char and Lee [11]. An unsteady natural convection in a horizontal annulus was investigated by Mizushima et al. [12]. Instability analyses for natural convection in horizontal annuli have been extensively addressed in the literature. Petrone et al. [13] numerically studied the linear instability of two-dimensional natural convection in air-filled horizontal annuli, and a map of possible flow patterns was established. Numerical results of the turbulent flow in a two-dimensional domain were presented by Farouk and Guceri [14]. In their work, the natural convection was considered in the annulus between two horizontal concentric cylinders. The stream-vorticity equation was discretized by finite difference techniques and turbulence was modeled by the $\kappa - \varepsilon$ approach for Rayleigh numbers above 105. The work by Char and Hsu [15] on turbulence modeling of natural convection in cylindrical horizontal annuli proposed a comparison of the different turbulence models, suggesting a better modeling practice. According to this paper, the non-linear model gives better results especially at higher Ra numbers. Padilla et al. [16] investigated laminar and unsteady natural convection at low Rayleigh number in a concentric annulus. Vafai and Ettefagh [17] performed a three-dimensional buoyancy-driven flow simulation in a closed horizontal annulus. They furnished a detailed analysis of the three-dimensional flow and temperature field. A comparative analysis of the Finite-Element (FEM) and Finite-Difference (FDM) Methods for solving the buoyancy-driven flow in two and three-dimensional annulus was done by Vafai and Desai [18]. By the time of their study, the computer memory saving was a must and the authors recommended the FEM in order to obtain fairly good results employing less computational resources. However, despite more expenses, the FDM was more suitable when a more detailed flow and temperature field information were needed. Numerical investigations of three-dimensional natural convection flow were accomplished by Yeh [19]. Lee [20] treated this problem over a good range of Rayleigh numbers allowing for both horizontal and vertical eccentricities of the inner cylinder. It was concluded that the mean Nusselt number increased with the Rayleigh number at a given angular velocity and decreased with the rotation speed while all other parameters being kept constant. Mixed convection of air between two horizontal concentric cylinders with a cooled rotating outer cylinder has been investigated by Yoo [21]. He categorized the flow field into three regions by the number of eddies formed in the concentric annulus (no, one and two eddy). Fusegi et al. [22] did not consider eccentric cases but treated the problem for both high and low values of the Froude number, σ, which expresses the relative magnitude of buoyancy versus rotation effects. Choudhury and Karki [23] studied this problem with the eccentricity along the vertical line. They concluded that the eccentricity introduces additional non-uniformity in the flow and temperature fields. Habib and Negm [24] numerically investigated the fully developed laminar mixed convection in horizontal concentric annuli for the case of non-uniform circumferential heating. Two heating conditions were explored, one in which the top half of the inner surface of the inner cylinder is uniformly heated while the bottom half is kept insulated, and the other in which the heated and the insulated surfaces were reversed. It was found that the bottom heating arrangement gives rise to a vigorous secondary flow, resulting in average Nusselt numbers much higher than those of pure forced convection. Nobari and Asgharian [25] investigated the three dimensional mixed convection in the vertical annulus using bipolar coordinate system, numerically. Most works for mixed convection problems in rotating systems have been performed for the flows in cylindrical annuli with vertical axe. Relatively few studies, however, have been done for the case of horizontal annuli. In most of the numerical studies on buoyancy driven flow in a horizontal annulus, the flow is assumed to be invariant in the axial direction, leading to a two-dimensional approach of the problem. However, in practical applications, the viscous shearing effects at the end walls could lead to erroneous results. Desai and Vafai [26] and Lee [27,28] with sufficiently long annulus and a range of limited parameters showed that there exists a core region with a certain Reynolds number, which can be approximated by a two-dimensional model.

Most heat transfer studies on the laminar mixed convection problem have been carried out using a staggered grid arrangement and stream function-vorticity, vorticity-velocity or primitive variables formulations based on the finite difference or finite element methods with the inner cylinder rotating. Lee et al. [29] used a generalized differential-integral quadrature discretization technique to solve a mixed convection problem inside horizontal eccentric annuli in a body-fitted coordinate system. In their study, they found out that the net circulation decreases and approaches zero with the rise of the Rayleigh number and it reaches its minimum value with high eccentricity when the inclination angle of eccentricity is π. Also authors Guj and Stella [30], Abu-Sitta et al. [31], Gakpe and Watkins [32], Mirza and Soliman [33] did experimental and numerical studies for investigating geometry, boundary condition, fluid properties, steady and unsteady effects in a concentric and eccentric annulus.

The present work deals with the flow and mixed convection in a horizontal eccentric annulus whose inner and outer walls are kept at hot and cold temper-

ature (T_h, T_c), respectively. Here, the two-dimensional full Navier-Stokes equations along with energy equation are solved in an orthogonal-structured grid of bipolar coordinate system employing a finite-volume method based on the SIMPLE algorithm. The bipolar coordinate system is a powerful tool for generating orthogonal grids, and implementation of boundary condition for eccentric problems is very simple in this manner. The only difficulties in bipolar coordinate system are growing up the equations, so that discretizing operation is time consuming. The solution of the full Navier-Stokes equations, using finite-volume method in the bipolar coordinate system for eccentric annulus, is carried out for the first time in this work.

2. Mathematical modelling

The geometry of the annulus is illustrated in Figure 1. The inner and outer cylinders are kept at hot and cold temperature (T_h, T_c), respectively. Both of the cylinders can rotate alone or simultaneously with a constant angular velocity. The continuity, momentum and energy equations, that describe the processes, are written in bipolar coordinate system for convenience. The two directions involved (ζ, η) are shown in Figure 2. The key feature of this coordinate system is

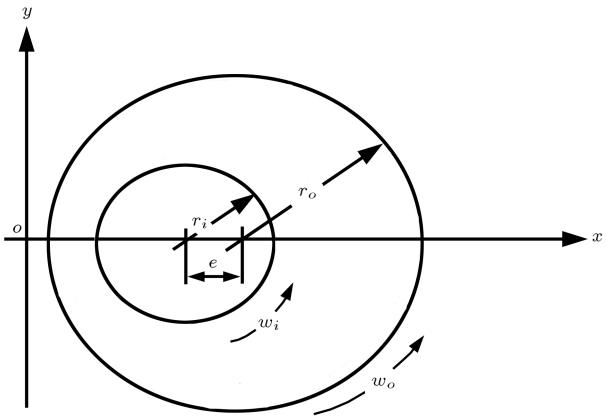

Figure 1. Geometry of annulus.

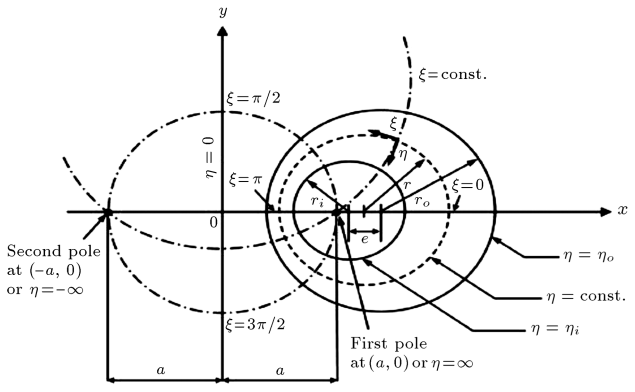

Figure 2. Bipolar coordinate system.

the orthogonality of the generated grid and its fitness to the physical domain which reduces the numerical errors stems from flux computing [25].

The transformation relations between the bipolar and Cartesian coordinate systems are as follows [25]:

$$E = \frac{e}{r_o - r_i}, \qquad N = \frac{r_i}{r_o}, \tag{1}$$

$$\eta_i = \cosh^{-1}((N(1+E^2)+(1-E^2))/(2NE)), \tag{2}$$

$$\eta_o = \cosh^{-1}((N(1-E^2)+(1+E^2))/(2E)), \tag{3}$$

$$a = r_i \sinh(\eta_i), \tag{4}$$

$$x = \frac{a\sinh\eta}{\cosh\eta - \cos\zeta}, \qquad y = \frac{a\sin\zeta}{\cosh\eta - \cos\zeta}, \tag{5}$$

where ζ varies from 0 to 2π and η varies over the range of $-\infty$ to ∞. As illustrated in Figure 2, the loci of the constant η lines are a set of circles whose centers are located on the x axis at the points $(\text{acot}(\eta), 0)$ and the loci of the constant ζ lines are circles whose radii are $a/\sin(\zeta)$ centered at the point $(0, \cot(\zeta))$ on the y axis. Constant η circles are utilized to generate eccentric cylinders, and the values of $\eta = \eta_i$ and $\eta = \eta_o$ represent the inner and outer cylinders, respectively.

Assuming Newtonian incompressible fluid in the presence of gravity, neglecting the radiation and viscous dissipation and using Boussinesqu approximation, the governing equations in the bipolar coordinate system can be written as [25]:

$$L = r_o - r_i, \qquad H = \frac{h_1}{L} = \frac{h_2}{L},$$

$$U_\zeta = \frac{u_\zeta L}{\upsilon}, \qquad U_\eta = \frac{u_\eta L}{\upsilon}, \tag{6}$$

$$P = \frac{pL^2}{\rho\upsilon^2}, \qquad \theta = \frac{T - T_c}{T_h - T_c}, \qquad \text{Pr} = \frac{\upsilon}{\alpha},$$

$$\text{Gr} = \frac{\beta g(T_h - T_c)L^3}{\upsilon^2}, \qquad \text{Nu} = hL/k. \tag{7}$$

Continuity

$$\frac{1}{H^2}\left[\frac{\partial}{\partial\zeta}(HU_\zeta) + \frac{\partial}{\partial\eta}(HU_\eta)\right] = 0. \tag{8}$$

ζ-momentum equation

$$\frac{1}{H^2}\left[\frac{\partial}{\partial\zeta}(HU_\zeta^2) + \frac{\partial}{\partial\eta}(HU_\zeta U_\eta)\right]$$

$$= -\frac{1}{H}\frac{\partial P}{\partial\zeta} + \frac{1}{H^2}\left[\frac{\partial^2 U_\zeta}{\partial\zeta^2} + \frac{\partial^2 U_\zeta}{\partial\eta^2}\right] + S_\zeta, \tag{9}$$

$$S_\zeta = \frac{1}{H^2}\frac{\partial H}{\partial \zeta}U_\eta^2 - \frac{1}{H^2}\frac{\partial H}{\partial \eta}U_\zeta U_\eta + \frac{2}{H^4}\frac{\partial H}{\partial \zeta}\frac{\partial H}{\partial \eta}U_\eta + \frac{2}{H^3}\frac{\partial H}{\partial \eta}\frac{\partial U_\eta}{\partial \zeta} - \frac{2}{H^4}\left(\frac{\partial H}{\partial \eta}\right)^2 U_\zeta + \frac{1}{H^3}\frac{\partial^2 H}{\partial \eta^2}U_\zeta + \frac{1}{H^3}\frac{\partial^2 H}{\partial \zeta^2}U_\zeta - \frac{2}{H^3}\frac{\partial H}{\partial \eta}\frac{\partial U_\zeta}{\partial \eta} - \left(\frac{\sinh\eta\sin\zeta}{\cosh\eta-\cos\zeta}\cos\phi + \frac{1-\cosh\eta\cos\zeta}{\cosh\eta-\cos\zeta}\sin\phi\right)\mathrm{Gr}x\theta. \quad (10)$$

η-momentum equation

$$\frac{1}{H^2}\left[\frac{\partial}{\partial \zeta}(HU_\zeta U_\eta) + \frac{\partial}{\partial \eta}(HU_\eta^2)\right] = -\frac{1}{H}\frac{\partial P}{\partial \eta} + \frac{1}{H^2}\left[\frac{\partial^2 U_\eta}{\partial \zeta^2} + \frac{\partial^2 U_\eta}{\partial \eta^2}\right] + S_\eta, \quad (11)$$

$$S_\eta = \frac{1}{H^2}\frac{\partial H}{\partial \eta}U_\zeta^2 - \frac{1}{H^2}\frac{\partial H}{\partial \zeta}U_\zeta U_\eta + \frac{2}{H^4}\frac{\partial H}{\partial \zeta}\frac{\partial H}{\partial \eta}U_\zeta + \frac{2}{H^3}\frac{\partial H}{\partial \zeta}\frac{\partial U_\zeta}{\partial \eta} - \frac{2}{H^4}\left(\frac{\partial H}{\partial \zeta}\right)^2 U_\eta + \frac{1}{H^3}\frac{\partial^2 H}{\partial \zeta^2}U_\eta + \frac{1}{H^3}\frac{\partial^2 H}{\partial \eta^2}U_\eta - \frac{2}{H^3}\frac{\partial H}{\partial \zeta}\frac{\partial U_\eta}{\partial \zeta} + \left(\frac{1-\cosh\eta\cos\zeta}{\cosh\eta-\cos\zeta}\cos\phi - \frac{\sinh\eta\sin\zeta}{\cosh\eta-\cos\zeta}\sin\phi\right)\mathrm{Gr}x\theta. \quad (12)$$

Energy equation

$$\frac{1}{H^2}\left[\frac{\partial}{\partial \zeta}(HU_\zeta\theta) + \frac{\partial}{\partial \eta}(HU_\eta\theta)\right] = \frac{1}{\mathrm{Pr}H^2}\left[\frac{\partial^2\theta}{\partial\zeta^2} + \frac{\partial^2\theta}{\partial\eta^2}\right]. \quad (13)$$

The dimensionless boundary conditions are:

$$\eta = \eta_i \rightarrow \theta = 1, \quad U_\eta = 0, \quad U_\zeta = \mathrm{Re}, \quad (14)$$

$$\eta = \eta_o \rightarrow \theta = 0, \quad U_\eta = 0, \quad U_\zeta = \mathrm{Re}_o. \quad (15)$$

Note that the kinematic viscosity has been used here to non-dimensionalize the velocity components. In this way the dimensionless velocity is changed to the Reynolds number which can be used for better interpretation of the results.

For eccentric annulus with rotating cylinders, the displacement of the inner cylinder introduces a throat region of the annulus which presents an obstruction to an otherwise free flow. The location and the size of the throat area, i.e. the orientation of the inner cylinder and the eccentricity, are the most critical factors in the analysis of eccentric configuration. Here, by changing the direction of gravity force (ϕ) we could model the effect of the eccentricity location, whereas the grid is fixed and the component of buoyancy force in the bipolar coordinate system is computed. These components can be seen in the S_ζ and S_η which are multiplied by $\mathrm{Gr}x\theta$. The details of the computational procedures have been presented in [34] where the scale factors and unit vectors are:

$$h_1 = h_2 = \frac{a}{\cosh\eta - \cos\zeta}, \quad (16)$$

$$h_1\hat{e}_\zeta = \frac{\partial x}{\partial \zeta}\hat{e}_x + \frac{\partial y}{\partial \zeta}\hat{e}_y, \quad (17)$$

$$h_2\hat{e}_\eta = \frac{\partial x}{\partial \eta}\hat{e}_x + \frac{\partial y}{\partial \eta}\hat{e}_y, \quad (18)$$

$$\hat{e}_\zeta = -\frac{\sinh\eta\sin\zeta}{\cosh\eta-\cos\zeta}\hat{e}_x - \frac{1-\cosh\eta\cos\zeta}{\cosh\eta-\cos\zeta}\hat{e}_y, \quad (19)$$

$$\hat{e}_\eta = \frac{1-\cosh\eta\cos\zeta}{\cosh\eta-\cos\zeta}\hat{e}_x - \frac{\sinh\eta\sin\zeta}{\cosh\eta-\cos\zeta}\hat{e}_y. \quad (20)$$

The distribution of the heat flux along the solid walls is examined through computing the local Nusselt number along the inner and outer cylinders:

$$\mathrm{Nu}_i(\zeta) = \left.\frac{\partial\theta}{\partial\eta}\right|_{\eta=\eta_i}, \qquad \mathrm{Nu}_o(\zeta) = \left.\frac{\partial\theta}{\partial\eta}\right|\eta = \eta_o. \quad (21)$$

The average inner and outer Nusselt numbers are given by:

$$\overline{Nu}_i = \frac{1}{2\pi}\int_0^{2\pi}\mathrm{Nu}_i(\zeta)d\zeta,$$

$$\overline{Nu}_0 = \frac{1}{2\pi}\int_0^{2\pi}\mathrm{Nu}_o(\zeta)d\zeta. \quad (22)$$

3. Numerical procedure

The finite-volume method, based on SIMPLE algorithm developed by Patankar [35], was used to solve the governing equations in the cylindrical bipolar system. Using this coordinate system has the privileges of orthogonal property and simplicity of computing different fluxes involved. This procedure in the present geometry was carried out for the first time in this study to the best of our knowledge. An easy method to generate the

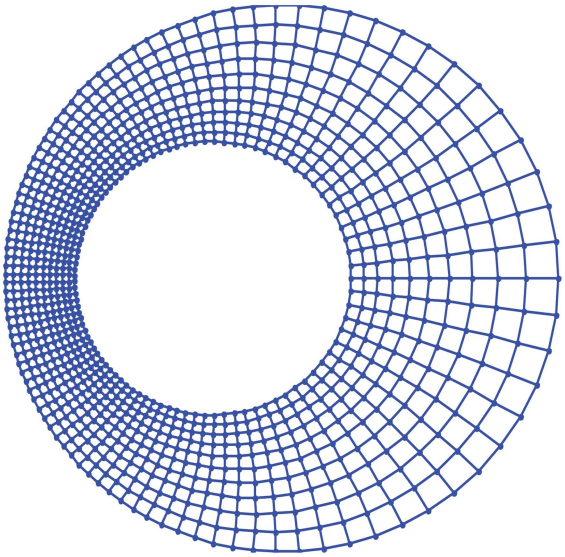

Figure 3. Physical grid.

Table 1. Grid independency (Ra = 1000, Re = 20, $E = 0.1$).

Cells	$\overline{\mathbf{Nu}}$	Deviation (%)
2000	1.5213	0
1000	1.5238	0.16
500	1.5311	0.4

grid is to divide all of the intervals into equal segments. If m and n represent the number of segments in ζ and η directions, respectively, then:

$$\Delta\zeta = \Delta\eta = \frac{2\pi}{m} = \frac{\eta_i - \eta_o}{n}. \tag{23}$$

In this manner, a uniform computational grid is obtained and numerical errors will be reduced. Because of the interdependency between the dimensions of the physical grid and the scale factor (h), which itself is a function of ζ and η, the corresponding physical grid will be highly smooth. The physical grid is shown in Figure 3.

The number of grids was checked. The deviations between the results obtained for different numbers of cells are shown in Table 1. Most of the runs considered here were done with 1000 cells. For high Rayleigh and Reynolds numbers (till 2×10^4 and 200, respectively) grid independency was checked too and was shown that using 1000 cells has reasonable accuracy (below 1%). A staggered grid was used to discretize the equations using power-law scheme. Face values were estimated by power law scheme for having realistic results. Since the source terms in ζ and η momentum equations are functions of the dependent variable, they have to be linearized with the central difference method. The alternating direction (implicit scheme) was used for generating system of algebraic equations; the resulting

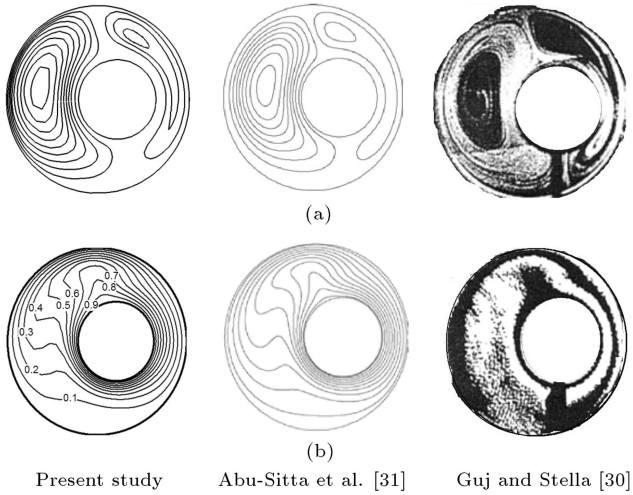

Figure 4. Comparison of results: (a) Streamlines and (b) isotherms; Ra = 5.3×10^3, Pr = 0.7, $E = 0.5$, $\sigma = \frac{2r_i}{r_o - r_i} = 1.47$.

tri-diagonal matrix was solved by a tri-diagonal matrix algorithm solver [36]. Here, the maximum error for the residuals was set to be of order of $O(10^{-5})$ for momentum and continuity equations. Also this value for energy equation was set to $O(10^{-8})$. It was shown that 3000 iterations were enough for all of the investigated values [35].

As it was stated in the Introduction, the steady-state solution can be extracted in the stable and unstable mode depending on effective parameters and the initial guesses. This work was done with the stability assumption, and validation was done with previous experimental and numerical works as follows.

The result of the present numerical work was verified against the experimental and numerical work of Kuehn and Goldstein [2], Guj and Stella [30], Abu-Sitta et al. [31] under pure natural-convection heat transfer cases. The findings of these comparisons were displayed in terms of streamlines, temperature contours and Nusselt number. As can be seen from Figures 4 and 5, the comparisons display excellent agreement between the tree studies.

4. Results and discussions

The overall objective of the current investigation was to explore the characteristics of the steady laminar mixed convection heat transfer in an eccentric annulus. All the results presented here were for $2r_i/L = 2$, where L is the gap width. Prandtl number throughout the paper was a constant and equal to 0.7 while Rayleigh number varied from 10^3 to 2×10^4. Both of the cylinders can rotate alone or simultaneously with a specific velocity for having mixed convection phenomenon. Note that positive sign is for counter clock-wise rotation and negative sign corresponds to clock-wise rotation.

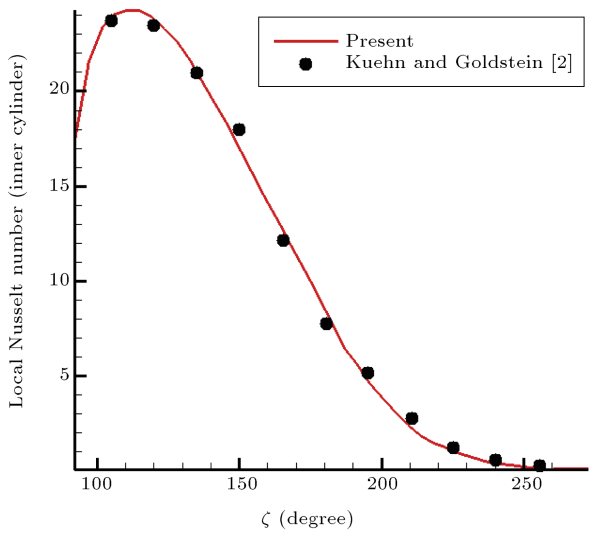

Figure 5. Comparison of results; Ra $= 5 \times 10^5$, Pr $= 0.7$, $E = 0.623$, $\sigma = \frac{2r_i}{r_o - r_i} = 1.2$.

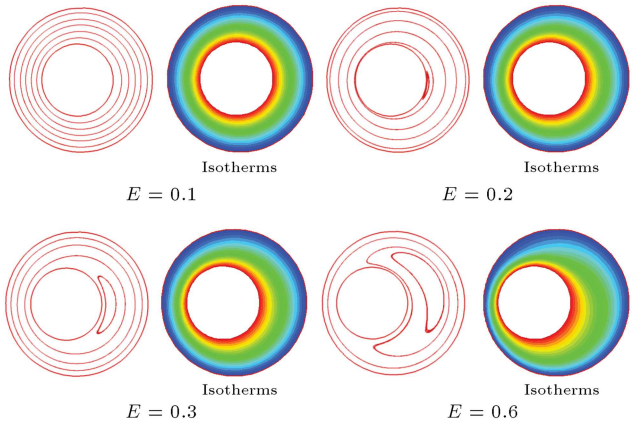

Figure 6. Eccentricity effect on forced convection ($\mathrm{Re}_o = 100$).

Results shown here are in the form of streamline and isotherm temperature which can be used for analyzing heat transfer and flow characteristics.

Streamlines with variation in eccentricity for pure forced convection are shown in Figure 6. Without eccentricity and concentric annulus, there is an analytical solution for the problem and the streamlines are concentric circles, but, as shown in this figure, increasing the amount of eccentricity produced an eddy in right hand of the annulus. This phenomenon can be explained by centrifugal forces. In the concentric case and at any radial position the centrifugal forces transmit from the same point which is the center of the cylinder while in the eccentric case they transmit from the center of a different circle. Confrontation between these forces which have different magnitude and trace causes eddy production in the right hand side of the annulus.

Eccentricity has considerable effect on Nusselt number. Mean Nusselt number on the inner cylinder for above configuration is show in Table 2. As shown, by increasing the eccentricity from 0.1 to 0.6, the Nusselt number increases from 1.4553 to 2.0000

Table 2. Mean Nusselt number on the inner cylinder for selected eccentricities.

E	0.0	0.1	0.2	0.3	0.6
$\overline{\mathrm{Nu}}$	1.4427	1.4553	1.4941	1.5619	2.0000

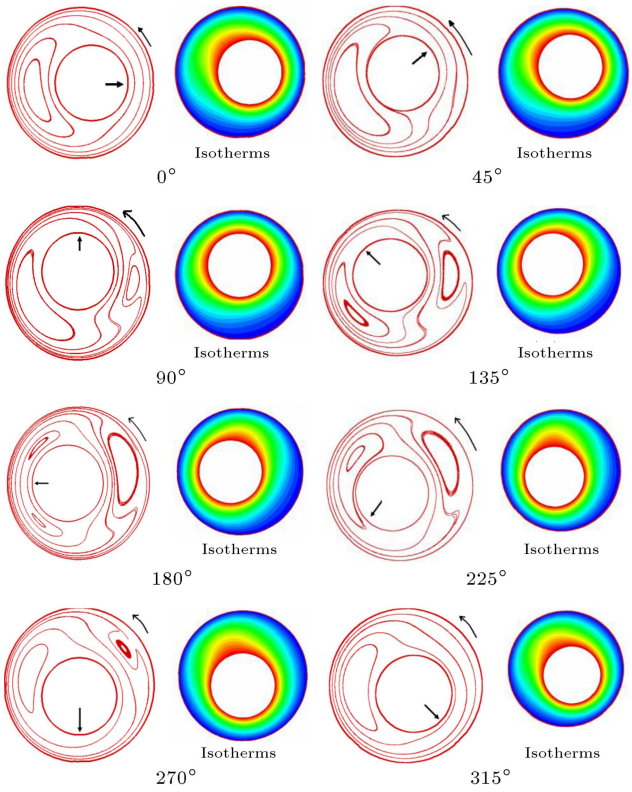

Figure 7. Streamlines and isotherms under different locations of eccentricity (Ra $= 1000$, $\mathrm{Re}_o = +20$, $E = 0.3$).

The orientation effect of eccentricity along with rotation of the outer cylinder with Reynolds number of +20 and Rayleigh number equal to 1000 is shown in Figure 7. As mentioned before, Rayleigh and Reynolds numbers are selected in a way that mixed convection phenomenon exists.

This idea can be checked by Richardson number as well which is defined by $\mathrm{Gr}/\mathrm{Re}^2$ and used for comparing between natural and forced convection problems [37]. The angles in counter clockwise direction given in the figures are related to the location of the throat area. In the case of 0° (throat area position is in the right side) only one eddy was generated at the left side. As throat position varied, another eddy was created in the right hand side, while in the left side, eddy was extended. In approximately 180°, the left side eddy was divided into two parts and we can see three eddies in the annulus, simultaneously. This

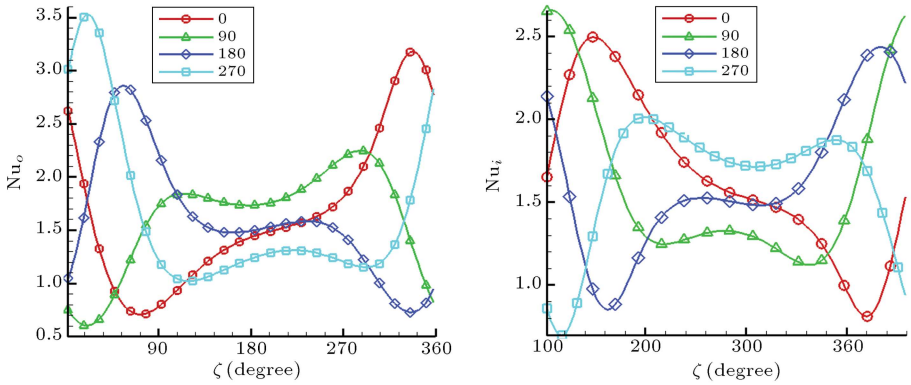

Figure 8. Location effect of eccentricity on local Nusselt number.

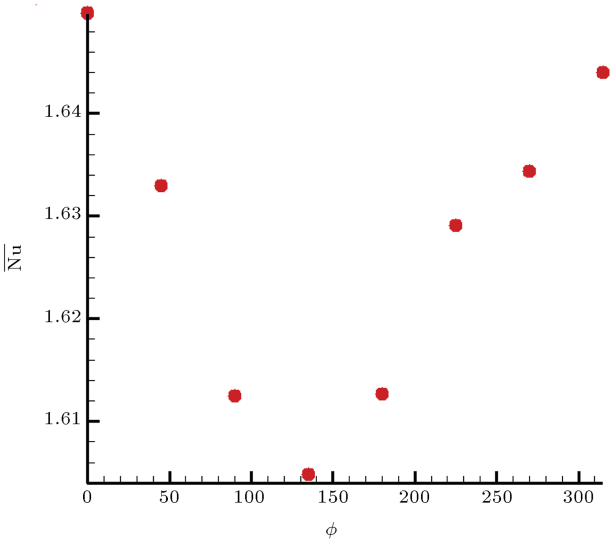

Figure 9. Location effect of eccentricity on mean Nusselt number.

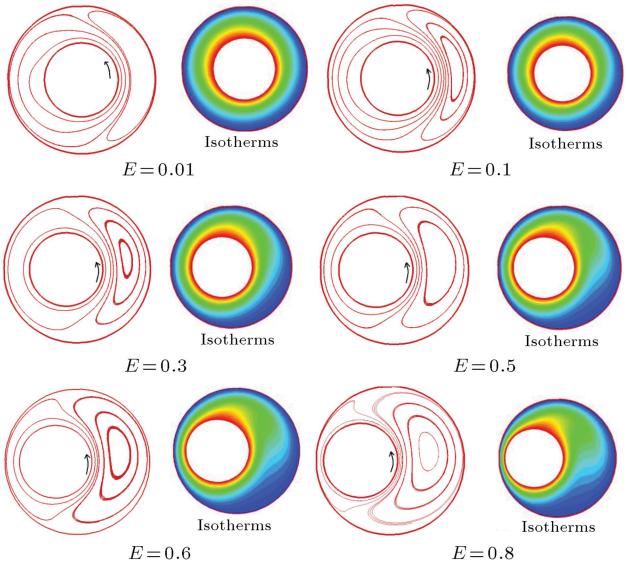

Figure 10. Streamlines and isotherms under different values of horizontal eccentricity (Ra = 1000, $Re_i = +20$).

phenomenon did not exist in the case of concentric annulus where in [21] mixed convection was categorized based on the number of eddies and the maximum of eddies was reported two in the concentric case. With the increase of the angle, the same pattern was repeated. The existence of the above mentioned eddies, which come in different numbers and positions, and are not the same in different situations, had considerable effect on the temperature distribution and heat transfer parameters. As can be seen, in all of the temperature contour cases, there is a maximum point, but the orientation of the larger eddy and direction of the flow rotation have direct effect on the place of this maximum point. This effect has been shown in Figures 8 and 9 in a better way. In Figure 8 the effect of the location of the throat area on the local Nusselt number is shown. This location not only changes the value of the maximum temperature but also has a considerable effect on the maximum magnitude of the Nusselt number. The greatest value of the Nusselt number in outer cylinder was observed in the case of 270° and its position and value were 20° and 3.52, respectively, while these values were 2.65 and 0° in the case of 90°, and for the inner cylinder.

In Figure 9, the effect of the location of the throat area on the mean Nusselt number is shown. Maximum and minimum values were 1.645 and 1.6048 and they were in the case of 0° and 135°, respectively. Also these values were compared with concentric case whose value is 1.5195.

Eccentricity effect when the inner cylinder rotates with dimensionless velocity ($Re_i = +20$) and Rayleigh number is assumed 1000 is shown in Figure 10. The eccentricity is horizontal and considered at 180°. For these conditions the forced convection flow was produced only by the inner cylinder. The eccentricity did not have a considerable effect on flow pattern, where one eddy was generated in all the cases and by increase of this eccentricity the eddy grew larger. Yet heat transfer characteristic experienced noticeable changes, where isotherms changed from concentric form to an eccentric form with a maximum temperature in the upper half. Effect of the eccentricity on the

Table 3. Mean Nusselt number.

E	0.01	0.1	0.3	0.5	0.6	0.8	0.9	0.95
$\overline{\mathbf{Nu}}$	1.5159	1.5336	1.6416	1.8501	2.0129	2.6537	3.5632	3.5633

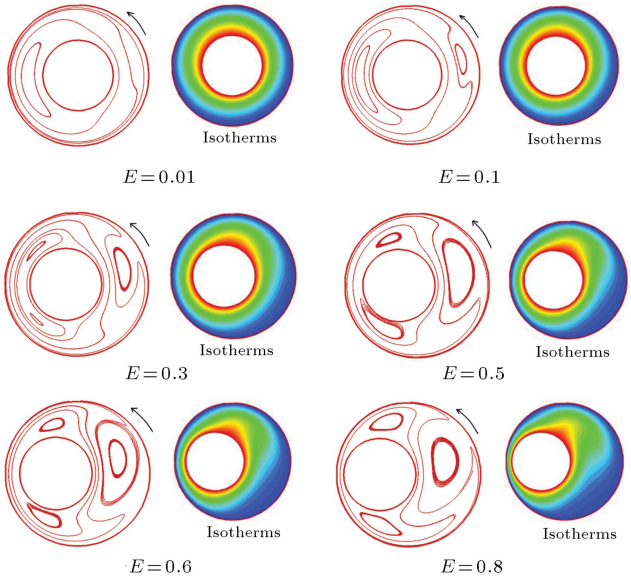

Figure 11. Streamlines and isotherms under different values of horizontal eccentricity (Ra = 1000, $\mathrm{Re}_o = +20$).

Table 4. Mean Nusselt number.

E	0.01	0.1	0.3	0.5	0.6	0.8
$\overline{\mathbf{Nu}}$	1.5188	1.5238	1.6127	1.8159	1.9785	2.6173

mean Nusselt number is shown in Table 3. Nusselt number increases from 1.5159 for $E = 0.01$ to 2.6537 for $E = 0.8$.

Effect of the increase of the eccentricity, when Ra = 1000 and the outer cylinder was rotating with a constant velocity of Re = +20, is shown in Figure 11. The condition applied here was similar to prior case, however, the difference was that the outer cylinder rotated and the results were completely different. When the eccentricity is small, one eddy can be seen in the left side while another one is in threshold of generating. With the increase of the eccentricity and because of the unbalanced centrifugal forces, the right hand eddy was produced and the left hand one was divided in a way that three independent eddies were generated at large values of eccentricity. These eddies causes high velocity gradients and considerable changes of heat transfer characteristics, such as isotherms and Nusselt number. The mean Nusselt number which changed from 1.5188 for $E = 0.01$ to 2.6173 for $E = 0.8$ is shown in Table 4.

Results under different kinds of rotation are presented in Figure 12. Rayleigh number and horizontal eccentricity were 1000 and 0.3, respectively. Both of the cylinders were rotating by Re = 10. First case is related to the counter clock-wise rotating of the cylinders. Rotation of both cylinders amplified velocity in the left-hand side and deleted eddy. In the second case, in which the outer and the inner cylinders were rotating counter clock-wise and clock-wise, respectively, the left hand side eddy was amplified. On the other hand, the eccentricity affects the eddy on the left-hand side, and after breaking it in two, the individual eddies were seen the same as before. The third case is related to the inner counter clock-wise and the outer clock-wise rotation of the cylinders. As it was mentioned above, here one large eddy was made in the right, and a small one in the left. In the last case, both of the cylinders were rotating clock-wise. Because of the reinforcement effect of rotating in the same direction, the left eddy was deleted completely and the right one got smaller. If the cylinders' velocity was increased, this one could be deleted, too. In the above cases, rotation of the cylinders in different directions did not have significant effects on the isotherms. This result was shown by mean Nusselt number at the inner and the outer cylinders in Figure 13.

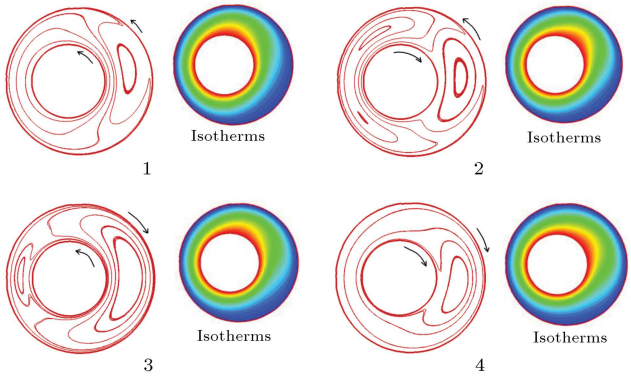

Figure 12. Streamlines and isotherms under different kind of rotations (Ra = 1000, $\mathrm{Re}_i = \pm 10$, $\mathrm{Re}_o = \pm 10$, $E = 0.3$).

When Rayleigh increases, natural convection or buoyancy force effect is increased. Here, Rayleigh's effect is investigated. The horizontal eccentricity (E) is supposed to be 0.3 when the outer cylinder is rotating by $\mathrm{Re}_o = +20$. When Rayleigh is increased, buoyancy forces increase and fluid near the inner cylinder can move as the velocity increases. As shown in Figure 14, at low Rayleigh number, three eddies could be seen simultaneously, where two of them were in the left and one was in the right. As Ra increased, the two eddies in the left were combined as they got wider, but the right one stayed almost the same. Increasing Ra caused considerable increase in the Nusselt number. Mean Nusselt number versus Rayleigh number is shown in

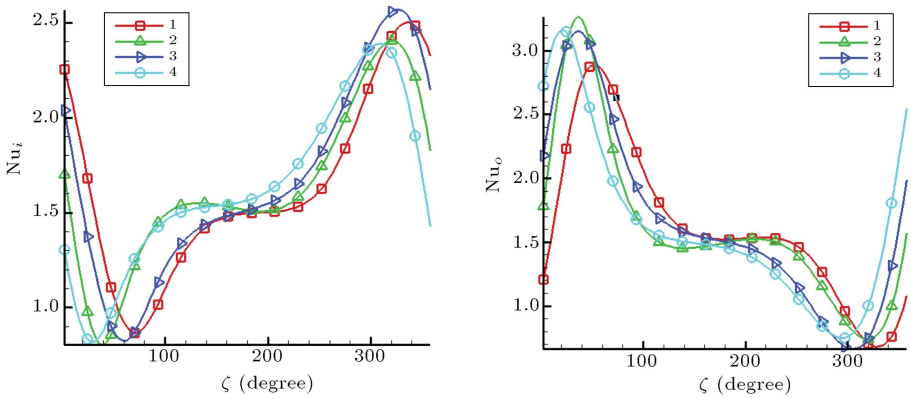

Figure 13. Local Nusselt number under different kinds of rotations.

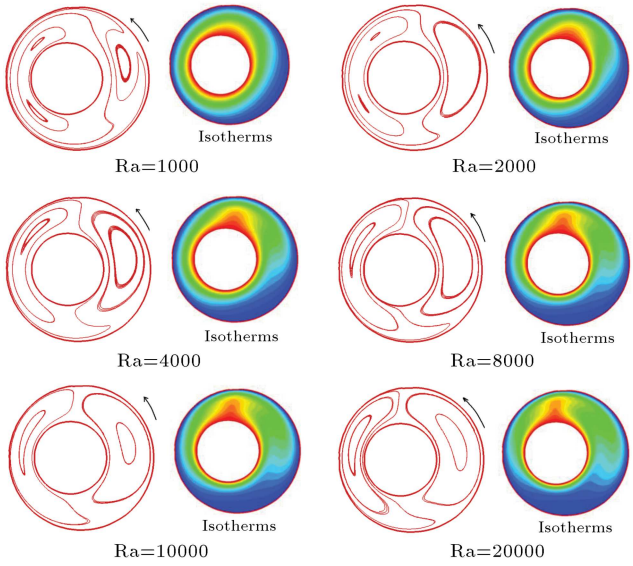

Figure 14. Streamlines and isotherms under different Rayleigh numbers ($E = 0.3$, $\mathrm{Re}_0 = 20$).

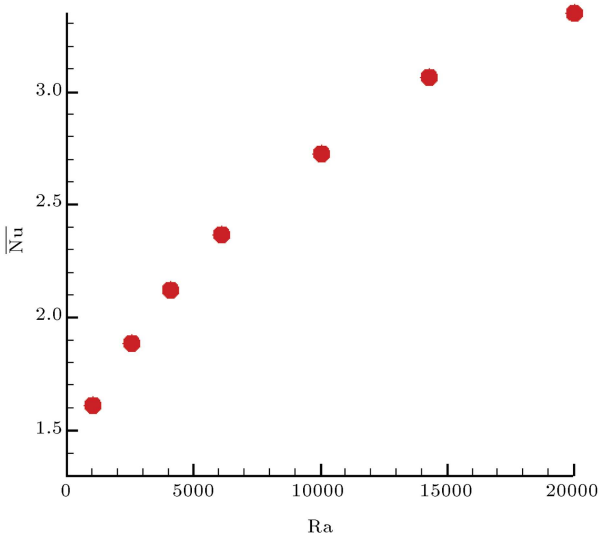

Figure 15. Mean Nusselt number versus Rayleigh number.

Figure 15. As can be seen, increasing Ra from 10^3 to 2×10^4 doubled the Nusselt number. Too much increase in Ra value caused cancellation of force convection and made flow pattern approach to natural convection unless if the cylinder's velocity was increased.

5. Conclusions

In the present study, the flow and heat transfer in horizontal eccentric annuli with rotating cylinders with constant angular velocities were investigated. Governing equations in the bipolar coordinate system were derived and solved by the finite volume method based on the SIMPLE algorithm. The overall and local heat transfer results were obtained from the numerically predicted temperature distributions. The main results and conclusions are as follows:

- The flow and heat transfer in eccentric configuration were strongly influenced by the orientation and eccentricity of the inner cylinder.
- The throat area presented an obstruction to an otherwise free flow, where not only the fluid flow was changed, but the temperature distribution and the local heat transfer coefficient were also affected.
- It was seen that the mean Nusselt number was increased with the increase of the eccentricity.
- Different kinds of rotation (clockwise and counter-clockwise) had strong effect on the flow and the heat transfer characteristics.

Nomenclature

a (m)	Location of the positive pole of the bipolar coordinate system, $r_i \sinh(\eta_i)$ or $r_o \sinh(\eta_o)$
e (m)	Eccentricity
E	Dimensionless eccentricity
g $\left(\frac{\mathrm{m}}{\mathrm{s}^2}\right)$	Acceleration of gravity
h	Convection coefficient

h_1 (m), h_2 (m)	Coordinate transformation scale factors, $a/(\cosh\eta - \cos\zeta)$
H	Dimensionless coordinate transformation factor
k	Conduction coefficient
L (m)	Gap width of the annulus, $r_o - r_i$
m	Number of grids in ζ direction
n	Number of grids in η direction
N	Radius ratio (r_i/r_o)
Nu	Nusselt number $= hL/k$
$\mathrm{Nu}_i, \mathrm{Nu}_o$	Local Nusselt numbers at the inner and outer cylinders, respectively, defined by Eq. (21)
$\overline{\mathrm{Nu}}$	Mean Nusselt number defined by Eq. (22)
Pr	Prandtl number, $\frac{\upsilon}{\alpha}$
Ra	Rayleigh number based on the gap width, $\frac{\beta g(T_h - T_c)L^3}{\upsilon\alpha}$
Gr	Grashof number, $\frac{\beta g(T_h - T_c)L^3}{\upsilon^2}$
r_i, r_o (m)	Radius of the inner and outer cylinders, respectively
$\mathrm{Re}_i, \mathrm{Re}_o$	Dimensionless velocity or Reynolds number at the inner and outer cylinders, respectively, $\left(\frac{u_\zeta L}{\upsilon}\right)$
S	Source term in momentum equations
p (Pa)	Pressure
P	Dimensionless pressure
T (K)	Temperature
T_h, T_c (K)	Temperatures at the inner and outer cylinders, respectively
u_ζ, u_η (m/s)	Velocity component in the ζ and η directions respectively
U_ζ, U_η	Dimensionless velocity component in the ζ and η directions respectively
x, y (m)	Coordinate variables in the cartesian coordinate system
ζ, η	Coordinate variables in the bipolar coordinate system
η_i, η_o	Values of η on the inner and outer cylinders, respectively
θ	Dimensionless temperature, $\frac{T - T_c}{T_h - T_c}$
$\upsilon \left(\frac{\mathrm{m}^2}{\mathrm{s}}\right)$	Kinematic viscosity
β (K^{-1})	Coefficient of thermal expansion
$\alpha \left(\frac{\mathrm{m}^2}{\mathrm{s}}\right)$	Thermal diffusivity
ϕ (radian)	Direction of buoyancy force
σ	Ratio of inner cylinder diameter to gap width (D_i/L)

References

1. Kuehn, T.H. and Goldstein, R.J. "An experimental and theoretical study of natural convection in the annulus between horizontal concentric cylinders", *Journal of Fluid Mechanics*, pp. 695-719 (1976).
2. Kuehn, T. and Goldstein, R. "An experimental study of natural convection heat transfer in concentric and eccentric horizontal cylindrical annuli", *J. Heat Transfer*, **100**, pp. 635-640 (1978).
3. Macleod, A.E. and Bishop, E.H. "Turbulent natural convection of gases in horizontal cylindrical annuli at cryogenic temperatures", *International Journal of Heat and Mass Transfer*, **32**, pp. 1967-1978 (1989).
4. Chai, J.C. and Patankar, S.V. "Laminar natural convection in internally finned horizontal annuli", *Numerical Heat Transfer, Part A*, **24**, pp. 67-87 (1993).
5. Desrayaud, G., Lauriat, G. and Cadiou, P. "Thermo convective instabilities in a narrow horizontal air-filled annulus", *Int. J. Heat Fluid Flow*, **21**, pp. 65-73 (2000).
6. Patankar, S.V., Ivanovic, M. and Sparrow, E.M. "Analysis of turbulent flow and heat transfer in internally finned tubes and annuli", *J. Heat Transfer*, **101**, pp. 29-37 (1979).
7. Rustum, I.M. and Soliman, H.M. "Numerical analysis of laminar mixed convection in horizintal internally finned tubes", *International Journal of Heat and Mass Transfer*, **33**, pp. 1485-1496 (1990).
8. Shahraki, F. "Modeling of buoyancy-driven flow and heat transfer for air in a horizontal annulus: Effects of vertical eccentricity and temperature-dependent properties", *Num. Heat Transfer*, **42**, pp. 603-621 (2002).
9. Dyko, M., Vafai, K. and Mojtabi, A. "A numerical and experimental investigation of stability of natural convective flows within a horizontal annulus", *J. Fluid Mech.*, **381**, pp. 27-61 (1999).
10. Alawadhi, E.M. "Natural convection flow in a horizontal annulus with an oscillating inner cylinder using Lagrangian-Eulerian kinematics", *Computers and Fluids*, **37**, pp. 1253-1261 (2008).
11. Char, M. and Lee, G. "Maximum density effect on natural convection of micro polar fluid between horizontal eccentric cylinders", *Int. J. Eng. Science*, **36**, pp. 157-69 (1998).
12. Mizushima, J., Hayashi, S. and Adachi, T. "Transitions of natural convection in a horizontal annulus", *International Journal of Heat and Mass Transfer*, **44**, pp. 1249-1257 (2001).
13. Petrone, G., Chenier, E. and Lauriat, G. "Stability of free convection in air filled horizontal annuli: influence

of the radius ratio", *International Journal of Heat and Mass Transfer*, **47**, pp. 3889-3907 (2004).

14. Farouk, B. and Guceri, S.I. "Laminar and turbulent natural convection in the annulus between horizontal concentric cylinders", *Journal of Heat Transfer*, **104**, pp. 631-636 (1982).
15. Char, M. and Hsu, Y.H. "Comparative analysis of linear and nonlinear low-Reynolds- number eddy viscosity models to turbulent natural convection in horizontal cylindrical annuli", *Numerical Heat Transfer*, **33**, pp. 191-206 (1998).
16. Padilla, E.L., Campregher, M.R. and Silveira-Neto, A. "Numerical analysis of the natural convection in horizontal annuli at low and moderate", *Thermal Engineering J.*, **5**(02), pp. 58-65 (2006).
17. Vafai, K. and Ettefagh, J. "An investigation of transient three-dimensional buoyancy-driven flow and heat transfer in a closed horizontal annulus", *International Journal of Heat and Mass Transfer*, **34**, pp. 2555-2570 (1991).
18. Vafai, K. and Desai, C.P. "Comparative analysis of the finite-element and finite-difference methods for simulation of buoyancy-induced flow and heat transfer in closed and open ended annular cavities", *Numerical Heat Transfer*, **23**, pp. 35-59 (1993).
19. Yeh, C. "Numerical investigation of the three-dimensional natural convection inside horizontal concentric annulus with specific wall temperature or heat flux", *International Journal of Heat and Mass Transfer*, **42**, pp. 775-84 (2002).
20. Lee, T.S. "Numerical computation of fluid convection with air enclosed between the annuli of eccentric heated horizontal rotating cylinders", *Int. J. Comput. Fluids*, **1**(3), pp. 355-368 (1992).
21. Yoo, J.S. "Mixed convection of air between two horizontal concentric cylinders with a cooled rotating outer cylinder", *International Journal of Heat and Mass Transfer*, **41**(2), pp. 293-302 (1998).
22. Fusegi, T., Farouk, B. and Enneth, S.B. "Mixed convection flows within a horizontal concentric annulus with a heated rotating inner cylinder", *Num. Heat Transfer*, **9**, pp. 591-604 (1986).
23. Choudhury, D. and Karki, K.C. "Laminar mixed convection in a horizontal eccentric annulus", *Num. Heat Transfer*, **22**, pp. 87-108 (1992).
24. Habib, M.A. and Negm, A.A. "Laminar mixed convection in horizontal concentric annuli with non-uniform circumferential heating", *Heat and Mass Transfer*, **37**, pp. 427-435 (2001).
25. Nobary, M.R.H. and Asgarian, A. "A numerical investigation of flow and mixed convection inside a vertical eccentric annulus", *Numerical Heat Transfer, Part A*, **55**, pp. 77-99 (2009).
26. Desai, C.P. and Vafai, K. "An investigation and comparative analysis of two- and three-dimensional turbulent natural convection in a horizontal annulus", *International Journal of Heat and Mass Transfer*, **37**, pp. 2475-2504 (1994).
27. Lee, T.S. "Numerical computation of fluid convection with air enclosed between the annuli of eccentric heated horizontal rotating cylinders", *Int. J. Comput. Fluids*, **1**(3), pp. 355-368 (1992).
28. Lee, T.S. "Numerical studies of mixed recirculatory flow in annuli of stationary and rotating horizontal cylinders with different radius ratios", *Int. J. Num. Methods Heat Fluid Flow*, **4**, pp. 561-573 (1994).
29. Lee, T.S., Hu, G.S. and Shu, C. "Application of GDQ method for study of mixed convection in horizontal eccentric annuli", *International Journal of Computational Fluid Dynamics*, **18**(1), pp. 71-79 (2004).
30. Guj, G. and Stella, F. "Natural convection in horizontal eccentric annuli: numerical study", *Num. Heat Transfer*, **27**, pp. 89-105 (1995).
31. Abu-Sitta, N.H., Khanafer, K., Vafai, K. and Al-Amiri, A.M. "combined forced and natural convection heat transfer in horizontally counterrotating eccentric and concentric cylinders", *Numerical Heat Transfer, Part A*, **51**, pp. 1167-1186 (2007).
32. Glakpe, E.K. and Watkins, J. "Effect of mixed boundary condition on natural convection in concentric and eccentric annular enclosure", *AIAA Paper*, pp. 1587-1591 (1987).
33. Mirza, S. and Soliman, H.M. "The influence of internal fins on mixed convection inside horizontal tubes", *Int. Commun. Heat Mass Transfer*, **12**, pp. 191-200 (1985).
34. Currie, I.G., *Fundamental Mechanics of Fluids*, McGraw-Hill, New York (1993-1994).
35. Patankar, S.V., *Numerical Heat Transfer and Fluid Flow*, McGraw-Hill, New York (1980).
36. Press, W.H., Flannery, B.P., Teukolsky, S.A., and Vetterling, W.T. *Numerical Recipes the Art of Scientific Computing*, Cambridge University Press, Cambridge (1986).
37. Incropera, F.P. and De Witt, D.A., *Introduction to Heat Transfer*, Third Edn., John Willy & Sons, New York (1996).

Biographies

Ahad Abedini was born in Tabriz, Iran, in 1982. He received his BS degree from Technical University of Shahrood in 2007, MS degree from Khajeh Nasir University in 2009, and PhD degree from Ferdowsi University of Mashhad in 2013, all in Mechanical Engineering. He is currently assistant professor in Department of Mechanical Engineering in Azad University of Semnan.

Asghar Baradaran Rahimi was born in Mashhad,

Iran, in 1951. He received his BS degree in Mechanical Engineering from Tehran Polytechnic in 1974 and his PhD degree in Mechanical Engineering from University of Akron, Ohio, U.S.A. in 1986. He has been professor in the Department of Mechanical Engineering at Ferdowsi University of Mashhad since 2001. His teaching and research interests include heat transfer and fluid dynamics, continuum mechanics, applied mathematics and singular perturbation.

Ali Kianifar was born in Mashhad, Iran in 1955. He received his BS degree in Mechanical Engineering from Thames Polytechnic, England in 1980 and PhD degree in Mechanical Engineering from Strathclyde University, U.K. in 1987. He has been Associate Professor in the Department of Mechanical Engineering at Ferdowsi University of Mashhad since 2009. His teaching and research interests include energy conversion, heat and mass transfer.